Available online at www.sciencedirect.com
ScienceDirect
Trans. Nonferrous Met. Soc. China 31(2021) 648−654
Transactions of Nonferrous Metals Society of China
www.tnmsc.cn

Superplastic forming characteristics of AZ41 magnesium alloy

S. TAYLOR[1], G. D. WEST[1], E. MOGIRE[2], F. TANG[1], H. R. KOTADIA[1]

1. WMG, the University of Warwick, Coventry CV4 7AL, UK;
2. Buehler, WMG Materials Engineering Centre, the University of Warwick, Coventry CV4 7AL, UK

Received 5 May 2020; accepted 30 November 2020

Abstract: An AZ41 magnesium alloy in the hot-rolled condition without further thermomechanical processing to modify its microstructure was investigated to establish its suitability for use within a superplastic forming process and to establish optimum forming parameters. Formability was assessed using elevated temperature tensile testing and hot gas bulging, across a range of strain rates (1×10^{-1}–1×10^{-3} s^{-1}) and temperatures (350−450 °C). Circle grid analysis with GOM Aramis cameras was used to understand peak strains and material thinning in relation to industrial forming processes. Post forming EBSD and STEM analysis was conducted to understand the mechanisms responsible for the materials formability, with dynamic recrystallization being clearly evident. Peak elongation of 520% was achieved at 450 °C and 1×10^{-3} s^{-1}; industrially relevant elongation was achieved at 1×10^{-2} s^{-1} at both 450 °C (195%) and 400 °C (170%).

Key words: magnesium; superplastic forming; superplasticity; electron back-scattered diffraction (EBSD); AZ41 magnesium alloy

1 Introduction

Magnesium has the lowest density ($\rho\approx1.74$ g/cm^3) among structural metals which, combined with its high specific stiffness, makes it a very attractive material for automotive manufacturers to aid in mass reduction to improve performance and efficiency [1]. Magnesium however suffers from limited ambient temperature ductility owing to its hexagonal close packed (HCP) crystal structure which offers limited slip systems with non-basal slip being extremely difficult. Elements such as aluminium and zinc are commonly alloyed with magnesium to improve mechanical properties but still ambient temperature formability is limited [2,3].

This limited ductility can be overcome through the use of advanced forming techniques such as superplastic forming (SPF) and quick plastic forming (QPF) which operate at elevated temperatures [4]. SPF typically takes place at temperatures around 70% of melting point of a material; at these temperatures, various mechanisms within material microstructure, such as grain boundary sliding (GBS) [5,6], dynamic recrystallization [7,8] and dislocation creep [9,10], allow for significant elongations greatly in excess of those at room temperature.

The superplastic properties of various magnesium alloys are well reported with studies showing elongation of up to 520% in AZ31 at 500 °C [11], 1000% in AZ91 under optimal conditions [12] and impressive 1604% at 300 °C following friction stir processing [13]. AZ31B alloy has been shown to be suitable for use within a QPF process which could significantly reduce industrial cycle times [14]. Magnesium alloys alloyed with rare earth (RE) elements have shown great promise as materials for SPF forming, and the elongation in

Corresponding author: S. TAYLOR; E-mail: scott.taylor.1@warwick.ac.uk
DOI: 10.1016/S1003-6326(21)65526-7

excess of 400% has been observed within WE43 which has a 3.4 wt.% RE addition due to solute drag [15]; other studies have shown impressive levels of formability in AE42 and QE22 RE-containing alloys [16]. In combination with advanced forming techniques, wrought magnesium alloys can see industrial applications in vehicle lightweighting, as shown by a General Motors demonstration part [14], and within the Porsche GT3 RS whose roof is superplastically formed from POSCO AZ31 alloy achieving a claimed 10 kg mass reduction [17].

In the present study, an AZ41 alloy was tested firstly by elevated temperature uniaxial tension to establish its strain rate sensitivity (m) value and suitability for SPF forming. Subsequently, the material was trialled within a free forming gas bulge test to investigate its formability on a larger more industrially relevant scale as a comparison to alloys currently used commercially. SEM and TEM analysis was employed to observe microstructures pre and post forming to understand the deformation mechanisms at work and to image the intermetallics within the alloy.

2 Experimental

In this study, a hot-rolled AZ41 alloy with alloying elements of 4.2 wt.% Al, 1.3 wt.% Zn and 0.3 wt.% Mn was investigated. The material was supplied in the as-rolled condition with a thickness of 3.3 mm; no further thermomechanical processing was applied prior to testing. Elevated temperature tensile testing was conducted using an Instron 5742 load frame with an integrated furnace and controlled using Instron Wave Matrix software operating in strain rate control to achieve constant strain rates throughout. Dog bone shaped samples were prepared by CNC machining; having a 15 mm gauge length and a nominal cross section of 9.4 mm^2. Tests were carried out across a range of strain rates from 1×10^{-1} to 1×10^{-3} s^{-1} and temperatures from 350 to 450 °C. Gas bulge testing was conducted using an Interlaken press; tests were conducted at 400 °C and GOM Aramis cameras were used to conduct circle grid analysis (CGA) using an established methodology [15].

Microstructural analysis was conducted using a JEOL 7800F FEGSEM and an Oxford instruments symmetry electron back-scattered diffraction (EBSD) camera. An accelerating voltage of 20 kV was used across all scans, with a step size of 0.2 μm. Samples were prepared using mechanical polishing regime modified from standard preparation techniques [18]; a final step of 30 min broad beam ion milling using a Hitachi IM4000 operating at 4 kV was applied to achieving a high quality surface finish. TEM samples were prepared by FIB lift-out using an FEI Scios dual beam FIB-SEM, with a viewing area size of approximately 6 μm × 6 μm and a nominal thickness of 0.15 μm. Samples were attached to a copper grid and analysed in an FEI Talos F200X FEG-(S)TEM operating at 200 kV. Scanning transmission electron microscopy (STEM) imaging and chemical maps were obtained using the four EDS Super-X Silicon Drift Detectors (SDD) fitted inside TEM Talos to identify the various intermetallics within the alloy.

3 Results and discussion

Elevated temperature tensile testing identified optimum conditions for maximum elongation as 1×10^{-3} s^{-1} and 450 °C where the material achieved 520% elongation, as illustrated in Fig. 1. Relatively uniform elongation was observed (Fig. 2) within the material with limited localised necking where failure occurred, indicative of typical SPF deformation occurring due to GBS complemented by dynamic recrystallization [19]. Decrease in forming temperature from 450 to 350 °C led to a significantly reduced peak elongation from 520% to 220%, as would be expected for such an alloy. Cup and cone failures and regions of localised necking were observed in lower temperature samples, indicating that dynamic recrystallization and GBS were not active. Increases in strain rate across all temperatures led to significant reductions in elongation due to the materials strain rate sensitivity and the reduced influence of mechanisms such as dynamic recrystallization at these strain rates.

Elongations of around 170% were achieved at 400 °C and 1×10^{-2} s^{-1} which is of industrial relevance as typical designs employing SPF techniques will obtain a maximum of elongation of 150% [20]. Testing across a full range of temperatures and strain rates allowed for m value of the materials to be established between 0.13 and

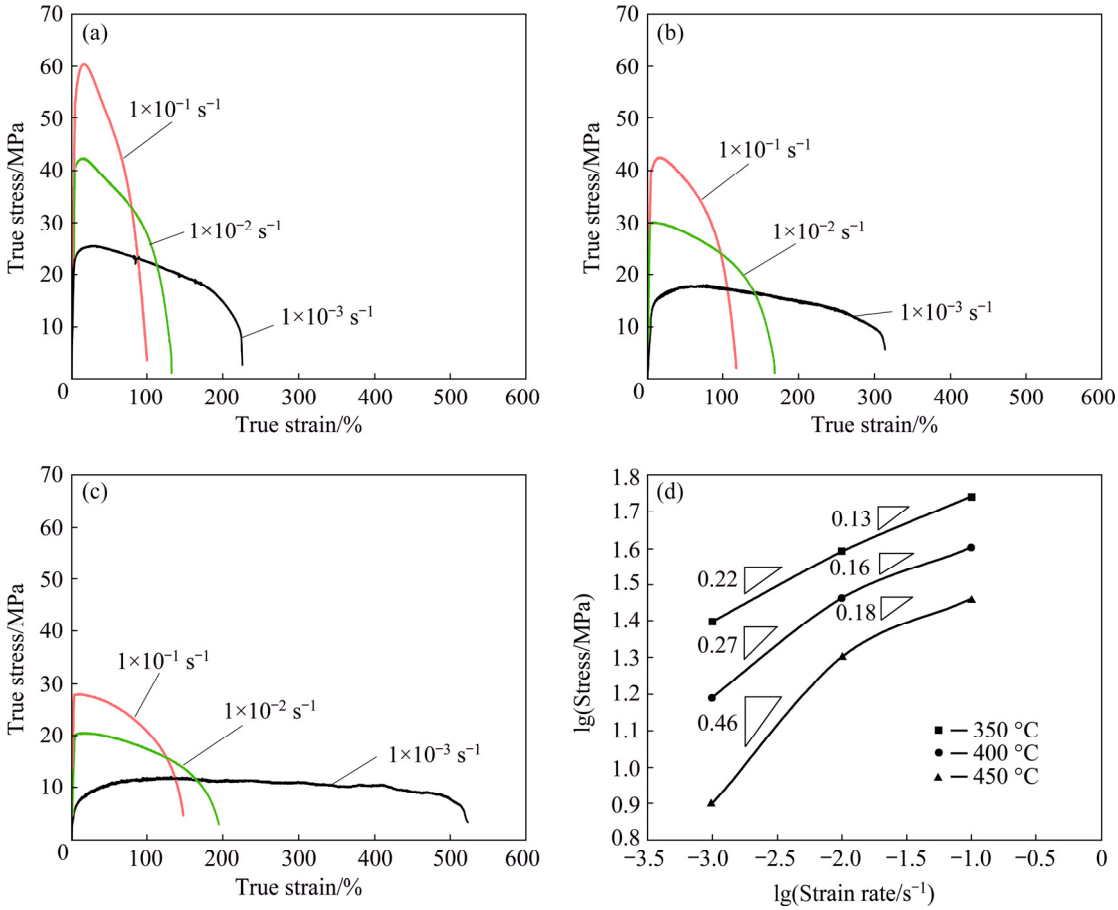

Fig. 1 Stress vs strain curves at 350 °C (a), 400 °C (b) and 450 °C (c), and *m* values of material across all temperatures at strain of 0.3 (d)

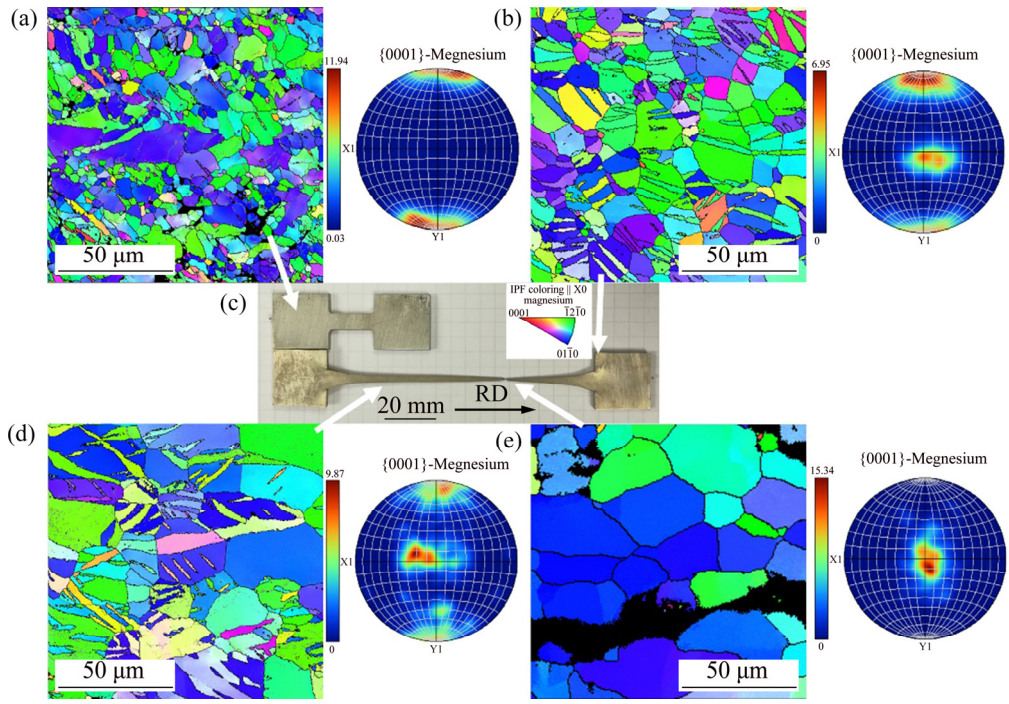

Fig. 2 IPF maps and MUD plots of as-received microstructure (a), microstructure in shoulder section after heating (b), dogbone geometry pre and post forming at 450 °C and 1×10^{-1} s^{-1} (c), microstructure in gauge length after heated deformation (d) and microstructure in failure region after heated deformation (e)

0.46, depending on forming condition, as shown in Fig. 1(d). The maximum m value of 0.46 being in the region where the stress exponent n=2 which, as discussed by SHELBY and WADSWORTH [21], indicates GBS as the dominate deformation mechanism. The m value being the materials strain rate sensitivity can be thought of, with its resistance to localised necking, higher resistance to localised necking being favourable for industrial forming. However, this alloy has not been investigated elsewhere; at the optimum temperature for this alloy (450 °C), elongations are in excess of those reported for AZ31 of 365% and 440%; AZ31 has a similar composition to the AZ41 in this study [22,23].

EBSD analysis of the material pre and post forming is shown in Fig. 2 alongside the dog bone geometry used for tensile testing. IPF maps were captured whilst multiples of uniform distribution (MUD) plots were from the same regions to capture more grains and give a sample set more representative of the full microstructure. Figure 2(a) shows the as-received hot-rolled AZ41 magnesium alloy microstructure prior to testing with some partially elongated grains in the direction of rolling, and very little evidence of annealing twins with a high MUD value of 11.9 is observed. In Fig. 2(b), when the alloy underwent heating but no physical deformation, an annealed structure is observed with grain twins dominating the microstructure, as expected due to magnesium alloys propensity to form annealing twins, and a reduction of MUD values to 6.9 indicates more random orientations within the microstructure. Within the gauge length in Fig. 2(d) exposed to heated deformation, we can see evidence of reduced numbers of grain twins, with independent strain-free grains being visible within the parent microstructure indicative of dynamic recrystallization during deformation. This

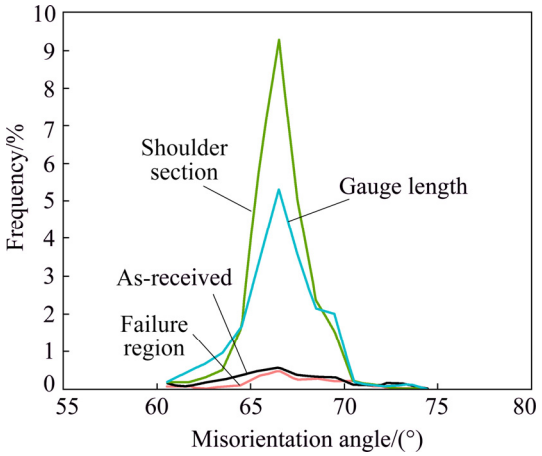

Fig. 3 Occurrences of high angle grain boundaries within AZ41 under different conditions

reduction in twinning is confirmed in Fig. 3 which shows a significant reduction in percentage of high angle grain boundaries within the structure. Towards the failure region of the sample shown in Fig. 2(e), we observe a grain structure devoid of twins, showing the dynamic recrystallization which has occurred throughout the testing, and an elongated structure is observed along with an increased MUD value of 15.3. Grain growth is clearly observed, which will lead to material softening, causing voids, the coalescence of which would be responsible for sample failure as observed at the bottom of the image [24,25].

Figure 4 illustrates the CGA strain map of a sample following gas bulge testing within a free forming bulge tool. A region of higher strain is observed near to the die entry, which has been observed in previous studies and is due to a combination of material thickness, tool entry angle and the free bulge of the test rather than being limited by tool walls [15]. Owing to this, the material was deformed to a specific height at various pressures to establish formability at higher strain rates; a dome height of 52 mm was achieved

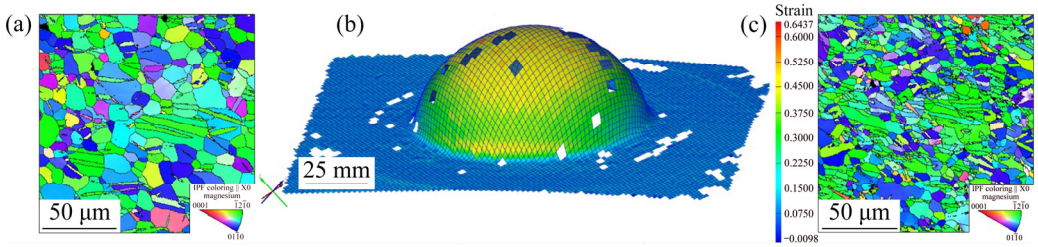

Fig. 4 IPF map of undeformed base after forming (a), circle grid analysis (CGA) strain analysis map of sample formed at 400 °C and 0.6 MPa (b), and IPF map of deformed section near to dome peak after forming (c)

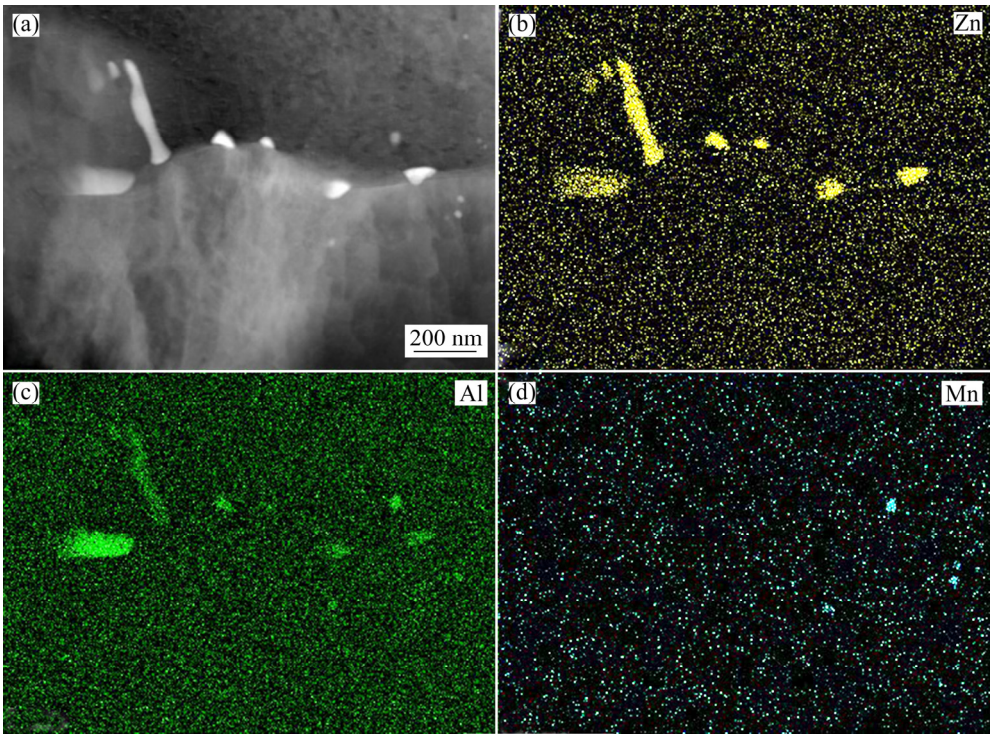

Fig. 5 Dark field STEM image of AZ41 alloy (a), with EDS maps showing zinc (b), aluminium (c) and manganese (d)

with strains of 0.49 at the dome peak with a forming time of around 12 min. Indicative of the materials ability to form, higher strain rates and lower forming temperatures are aspects of the SPF forming process, which are inhibitive to its uptake across more industrial applications.

The equivalent strain at the dome peak was 115%; equivalent strain being a measure of strain within a material due to thinning is calculated by $((T_o/T_s)-1)\times100\%$, where T_o is original thickness and T_s is strained thickness. Being a measure of material thinning this is an important factor within the design of parts formed within SPF processes. A finer microstructure is observed in Fig. 4(c) compared to Fig. 4(a), indicating that grain growth has occurred within the undeformed base material, whilst the same dynamic recrystallization mechanism observed in Fig. 2(e) was also active within the bulged sample.

Premature melting of aluminium intermetallics $Al_{12}Mg_{17}$ is reported to be responsible for premature failures within AZ91 alloys, due to melting at and around the material forming temperature [26]. STEM EDS analysis was conducted to understand the location and composition of intermetallics within the AZ41 in this study, and the resultant dark field image and EDS maps are shown in Fig. 5. Zn and Al containing intermetallics were observed to decorate grain boundaries with a maximum size of around 200 nm, and this size is too large to aid recrystallization by means of particle stimulated nucleation, but will inhibit grain growth following dynamic recrystallization, helping to minimize localised necking. Manganese intermetallics were observed within the matrix of grains but not across grain boundaries. Due to the lower aluminium content in this alloy compared to AZ91, less $Al_{12}Mg_{17}$ intermetallics are observed, suggesting that they will have less influence on the failure of the material, which occurs due to coalescence of voids at extreme elongations.

4 Conclusions

(1) Superplastic behaviour was observed within the AZ41 alloy, with peak elongation in excess of 500% under the optimum forming conditions. Optimum forming conditions were identified as 450 °C and 1×10^{-3} s^{-1}.

(2) The material was capable of achieving industrially relevant levels of formability under sub optimum conditions with 170% elongation achieved at 400 °C and 1×10^{-2} s^{-1}. At 400 °C within a gas bulge test, the material achieved a dome height of

52 mm in around 12 min, similar to that of high strength aluminium under the same conditions.

(3) Grain boundary sliding was the primary deformation mechanism responsible for super-plasticity, with clear evidence of dynamic recrystallization of the microstructure. No evidence of solute drag or dislocation creep was observed during forming.

Acknowledgments

The authors would like to thank the WMG High Value Manufacturing Catapult Centre for funding this work. In addition, the characterisation facility is supported from the Higher Education Funding Council for England (HEFCE).

References

[1] HIRSCH J, AL-SAMMAN T. Superior light metals by texture engineering: Optimized aluminum and magnesium alloys for automotive applications [J]. Acta Materialia, 2013, 61(3): 818−843.

[2] PEKGULERYUZ M O. Current developments in wrought magnesium alloys [C]//Advances in Wrought Magnesium Alloys. Elsevier, 2012.

[3] TRANG T T T, ZHANG J H, KIM J H, ZARGARAN A, HWANG J H, SUH B C, KIM N J. Designing a magnesium alloy with high strength and high formability [J]. Nature Communications, 2018, 9(1): 1−6.

[4] GRIMES R. Superplastic forming of magnesium alloys [C]//Superplastic Forming of Advanced Metallic Materials. Elsevier, 2011.

[5] CHOKSHI A H, MUKHERJEE A K, LANGDON T G. Superplasticity in advanced materials [J]. Materials Science and Engineering R, 1993, 10(6): 237−274.

[6] TAN J C, TAN M J. Superplasticity and grain boundary sliding characteristics in two stage deformation of Mg−3Al−1Zn alloy sheet [J]. Materials Science and Engineering A, 2003, 339: 81−89.

[7] MOHRI T, MABUCHI M, NAKAMURA M, ASAHINA T, IWASAKI H, AIZAWA T, HIGASHI K. Microstructural evolution and superplasticity of rolled Mg−9Al−1Zn [J]. Materials Science and Engineering A, 2000, 290: 139−144.

[8] MOHAMED F A, LANGDON T G. The transition from dislocation climb to viscous glide in creep of solid solution alloys [J]. Acta Metallurgica, 1974, 22(6): 779−788.

[9] KULAS M A, GREEN W P, TALEFF E M, KRAJEWSKI P E, MCNELLEY T R. Deformation mechanisms in superplastic AA5083 materials [J]. Metallurgical and Materials Transactions A: Physical Metallurgy and Materials Science, 2005, 36(5): 1249−1261.

[10] HIRAI K, SOMEKAWA H, TAKIGAWA Y, HIGASHI K. Superplastic forging with dynamic recrystallization of Mg−Al−Zn alloys cast by thixo-molding [J]. Scripta Materialia, 2007, 56(3): 237−240.

[11] DASHWOOD R J, KLAUMUNZER D, JACKSON M, FAN Z Y, GRIMES R. The development of superplastic magnesium alloy sheet [J]. Key Engineering Materials, 2010, 433: 273−279.

[12] SOLBERG J K, TØRKLEP J, BAUGER Ø, GJESTLAND H. Superplasticity in magnesium alloy AZ91 [J]. Materials Science and Engineering A, 1991, 134: 1201−1203.

[13] ZHANG D T, WANG S X, QIU C, ZHANG W. Superplastic tensile behavior of a fine-grained AZ91 magnesium alloy prepared by friction stir processing [J]. Materials Science and Engineering A, 2012, 556: 100−106.

[14] VERMA R, CARTER J T. Quick plastic forming of a decklid inner panel with commercial AZ31 magnesium sheet [J]. SAE Technical Papers, 2006−01−0525. https://doi.org/10.4271/2006−01−0525.

[15] TAYLOR S, JANIK V, GRIMES R, MOGIRE E, DASHWOOD R. Comparison of superplastic forming abilities of as-cast AZ91 magnesium alloy prepared by twin roll casting and WE43 magnesium alloy [J]. Materialwissenschaft und Werkstofftechnik, 2018, 49(10): 1206−1212.

[16] TROJANOVÁ Z, DROZD Z, LUKÁČ P. Superplastic behaviour of selected magnesium alloys [M]//Magnesium Alloys - Selected Issue. IntechOpen, 2018. Doi:10.5772/intechopen.79752

[17] POSCO to supply magnesium sheets for Porsche's new model roof [Z]. 2015. https://worldindustrialreporter.com/posco-to-supply-magnesium-sheets-for-porsches-new-model-roof/

[18] van der VOORT G. Tech notes: Metallography of magnesium and its alloys, Volume 4, Issue 2 https://www.buehler.cn/solutions/technotes/vol4_issue2.pdf (accessed 26.02.20)

[19] RIDLEY N. Metals for superplastic forming [M]//Superplastic Forming of Advanced Metallic Materials. Elsevier, 2011: 3−33.

[20] EDWARDS D. Ground-breaking design freedom from high strength 7000 series aluminium alloys [C]//Global Automotive Lightweight Materials. Detroit, 2016. https://www.galmintelligence.com/c547/global-automotive-lightweight-materials-detroit-2016/

[21] SHERBY O D, WADSWORTH J. Superplasticity−Recent advances and future directions [J]. Progress in Materials Science, 1989, 33(3): 169−221.

[22] ZHANG K F, YIN D L, WANG G F, HAN W B. Superplastic deformation behavior of hot-rolled AZ31 magnesium alloy sheet at elevated temperatures [J]. Journal of Wuhan University of Technology: Materials Science Edition, 2006, 21(3): 1−6.

[23] CUSICK M, ABU-FARHA F, LOURS P, MAOULT Y, BERNHART G, KHRAISHEH M. Superplastic forming of AZ31 magnesium alloy with controlled microstructure [J]. Materialwissenschaft und Werkstofftechnik, 2012, 43(9): 810−816.

[24] CAMPBELL J. Cavitation during superplastic forming [J]. Materials, 2011, 4(7): 1271−1286.

[25] BLANDIN J J. Superplastic forming of magnesium alloys: Production of microstructures, superplastic properties, cavitation behaviour [J]. Materials Science Forum, 2007, 551: 211−217.

[26] SRINIVASAN A, AJITHKUMAR K K, SWAMINATHAN J, PILLAI U T S, PAI B C. Creep behaviour of AZ91 magnesium alloy [J]. Procedia Engineering, 2013, 55: 109−113.

AZ41 镁合金超塑性成形特性

S. TAYLOR[1], G. D. WEST[1], E. MOGIRE[2], F. TANG[1], H. R. KOTADIA[1]

1. WMG the University of Warwick, Coventry CV4 7AL, UK;
2. Buehler, WMG Materials Engineering Centre, the University of Warwick, Coventry CV4 7AL, UK

摘　要：研究 AZ41 镁合金在热轧(无后续热变形)条件下的显微组织变化，以确定其在超塑性成形工艺中的适用性，并确定最佳成形参数。采用高温拉伸试验和热气体胀形试验对材料在不同应变速率(1×10^{-1}~1×10^{-3} s^{-1})和温度(350~450 °C)下的成形性进行评估。利用 GOM Aramis 相机进行圆形网格分析，了解峰值应变和材料减薄与工业成形过程的关系。通过成形后 EBSD 和 STEM 分析材料成形性的机制，发现存在明显动态再结晶。最佳成形参数为 450 °C 和 1×10^{-3} s^{-1}，此时的峰值伸长率达 520%。在 1×10^{-2} s^{-1} 下，450 °C 和 400 °C 时的工业相关伸长率分别为 195%和 170%。

关键词：镁；超塑性成形；超塑性；电子背散射衍射(EBSD)；AZ41 镁合金

(Edited by Bing YANG)